Decaying grid-generated turbulence in a rotating tank

C. Morize, F. Moisy,[a] and M. Rabaud
Fluides, Automatique et Systèmes Thermiques, Bâtiment 502, Campus Universitaire, 91405 Orsay Cedex, France

(Received 17 December 2004; accepted 19 July 2005; published online 16 September 2005)

The decay of initially three-dimensional homogeneous turbulence in a rotating frame is experimentally investigated. Turbulence is generated by rapidly towing a grid in a rotating water tank, and the velocity field in a plane perpendicular to the rotation axis is measured by means of particle image velocimetry. During the decay, strong cyclonic coherent vortices emerge, as the result of enhanced stretching of the cyclonic vorticity by the background rotation, and the selective instability of the anticyclonic vorticity by the Coriolis force. This asymmetry towards cyclonic vorticity grows on a time scale Ω^{-1} (Ω is the rotation rate), until the friction from the Ekman layers becomes dominant. The energy spectrum perpendicular to the rotation axis becomes steeper as the instantaneous Rossby number $\mathrm{Ro}_\omega = \omega'/2\Omega$ decreases below the value 2 ± 0.5 (ω' is the root-mean square of the vertical vorticity). The spectral exponent increases in time from its classical Kolmogorov value 5/3 up to values larger than 2. Below the threshold $\mathrm{Ro}_\omega < 2$, the velocity derivative skewness decreases as $|S| \propto \mathrm{Ro}_\omega$, reflecting the inhibition of the energy transfers by the background rotation, with a net inverse energy cascade that develops at large scales. © *2005 American Institute of Physics*. [DOI: 10.1063/1.2046710]

I. INTRODUCTION

Turbulence subjected to system rotation is present in a wide range of applications, from engineering to geophysics and astrophysics.[1–3] Although often coupled to other effects, such as stratification or confinement, rotating turbulence in itself is a delicate issue that is not completely understood. Rotation considerably affects the dynamics and the structure of turbulence through the Coriolis force, which tends to two-dimensionalize the flow. The importance of rotation is usually measured from the Rossby number, $\mathrm{Ro} = U/\Omega L$, where U is a typical velocity, L is a typical length scale, and Ω is the rotation rate. While the two-dimensional (2D) state is expected in the limit $\mathrm{Ro} \to 0$, according to the Taylor-Proudman theorem, the two-dimensionalization process itself, being driven by the nonlinear interactions, requires moderate Rossby numbers or asymptotically large times to take place. Such asymptotic may however never be reached in laboratory experiments, for which a much shorter time scale associated to the dissipation in the Ekman layers is present,[1] which may prevent this slow trend towards two-dimensionality.

Early experiments, either from an oscillating grid or source-sink forcing in a rotating frame,[4–7] or from a wind tunnel with a rotating honeycomb,[8] have led to a base of commonly accepted features for rotating turbulence. First, the flow develops a strong anisotropy, which may be characterized from increased correlation lengths along the axis of rotation.[8] This first observation is in qualitative agreement with a trend towards 2D turbulence, except that the flow is found to become dominated by a population of large-scale coherent cyclonic vortices,[5,6] while symmetric vorticity fluctuations are expected for strictly 2D turbulence. Second, the energy transfer from large to small scales is reduced, leading to reduced energy dissipation and a slower decay.[8] This inhibition of the energy transfer may however be hidden for bounded flows, for which the Ekman friction leads to an extra dissipation.[4,9]

The asymmetry between cyclonic and anticyclonic vorticity is a generic property of rotating systems, which originates from a selective destabilization of the anticyclonic vorticity by the Coriolis force when $\mathrm{Ro} \simeq O(1)$.[10–12] The statistical signature of this asymmetry has been first characterized for decaying rotating turbulence by Bartello *et al.*[13] from large-eddy simulations (LES), showing that the vorticity skewness at a fixed time during the decay was maximum for an initial Rossby number $\sim O(1)$. As a consequence, the vorticity distribution in the two-dimensionalization process is expected to be strongly affected by the initial conditions in the decaying case, or the forcing scheme in the stationary case, and should not be universal.

The trend towards two-dimensionality may be characterized in the spectral space by a net energy transfer toward wave vectors $\mathbf{k}$ normal to the rotation axis.[14,15] This trend towards two-dimensionality is not directly related to a trend towards a two-component flow, as may be traced by the anisotropy of the Reynolds stress tensor.[14,16,17] Despite much theoretical and numerical efforts, the issues of the direction of the energy transfers towards smaller or larger wavenumber magnitude $k = |\mathbf{k}|$, and the shape of the energy spectrum, remain controversial. First, a simple dimensional analysis, assuming that Ω^{-1} is the only relevant time scale in the problem and no energy transfer takes place, yields a spectrum $E(k) \sim \Omega^2 k^{-3}$ (e.g., Smith and Waleffe[18]). Although similar to that of geostrophic turbulence (Charney[19]) and strictly 2D turbulence in the enstrophy cascade regime,[20] this

[a]Electronic mail: moisy@fast.u-psud.fr

k^{-3} spectrum in itself does not prove that rapidly rotating turbulence actually tends towards a purely 2D state. On the other hand, assuming local energy transfers and taking Ω^{-1} as the time scale for those transfers, but ignoring anisotropic effects, a k^{-2} spectrum has been derived by Zhou[21] and Canuto and Dubovikov,[22] with some support from simulations[23,24] and experiments at a moderate Rossby number.[25] Attempts to derive the three-dimensional (3D) anisotropic spectrum have been recently carried out by Galtier[26] and Cambon *et al.*[27] in the limit of a quasizero Rossby number. Steeper slopes, $k^{-5/2}$ to k^{-3}, are obtained by these authors, which are in qualitative agreement with direct numerical simulation (DNS),[18,28] LES,[29] and numerical integration of an asymptotic quasinormal Markovian (QNM) closure model.[30]

Recently, particle image velocimetry (PIV), by offering the possibility to study the spatial structure of the flow as well as multipoint statistics, renewed the interest for rotating turbulence experiments.[25,31,32] In particular, the flow field in the plane normal to the rotation axis can be obtained from this measurement technique, in contrast with more conventional one-point probes that are usually restricted to measurements along the rotation axis. Baroud *et al.*[25] observed a transition towards quasi-2D turbulence in an experiment where forcing was applied at small scale through a circular set of 120 jets in a rotating annulus. These authors observed a flow dominated by large-scale coherent vortices, which was interpreted in terms of an inverse energy cascade associated to a k^{-2} spectrum, different from the Kolmogorov-Kraichnan scaling $k^{-5/3}$ for exact 2D turbulence.[33] In recent experiments using the large-scale "Coriolis" rotating platform, Praud *et al.*[32] have investigated the decaying 2D turbulence in the presence of rotation and stratification. In these experiments, turbulence was generated by towing a rake in the direction perpendicular to the rotation, thus preferentially forcing the horizontal modes of the flow. Energy spectra k^{-3} were obtained, in agreement with the expected 2D state in the enstrophy cascade regime. These experiments gave evidence of the existence and stability of a suitably forced 2D turbulence state in a rotating and stratified system, but do not address the issue of the convergence towards this 2D state from a 3D isotropic forcing.

The present experiment has been specially designed to investigate the influence of background rotation during the free decay of an otherwise initially 3D homogeneous and isotropic turbulence. Turbulence is generated by rapidly towing a grid in a rotating water tank, providing an initial state that is close to the ideal situation of homogeneity and isotropy. The setup is similar to the ones proposed by Hopfinger *et al.*[6] or Dickinson and Long,[7] which made use of an oscillating grid in a rotating tank. The advantage of their system was to provide a stationary forcing, but its main drawback was to produce a strongly inhomogeneous flow, with essentially 3D turbulence close to the grid and quasi-2D turbulence at the other end of the tank. In our experiment, close to the one originally proposed by Ibbetson and Tritton,[4] the grid is initially towed through the whole height of the tank and the turbulence freely decays, so that the background rotation gradually affects the entire flow in an homogeneous way. In that sense, the present experiment is closer to the theoretical and numerical approaches, for which homogeneity is generally required while stationarity is not.

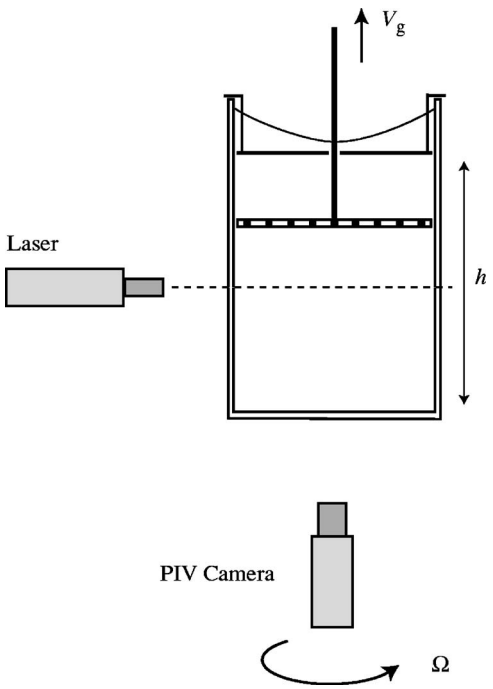

FIG. 1. Schematic of the experimental setup. The water tank, the grid, and the camera are in the rotating frame, while the laser is in the laboratory frame.

The paper is organized as follows: In Sec. II the experimental setup and the particle image velocimetry is presented. Statistics of the vorticity field are presented in Sec. III, with particular attention paid to the asymmetry between cyclonic and anticyclonic vorticity in the course of the decay. Power spectra are investigated in Sec. IV, and the influence of the Rossby number on the energy transfers is characterized from the velocity derivative skewness in Sec. V. Finally, some concluding remarks are offered in Sec. VI.

II. EXPERIMENTAL SETUP

A. Experimental apparatus

The experimental setup is sketched in Fig. 1. It consists of a water-filled square glass tank, 55 cm in height and 35 cm in side length, mounted on a rotating turntable, whose angular velocity Ω has been varied between 0.13 and 4.3 rad s^{-1} (see Table I for a summary of the flow parameters). By convention the rotation axis is directed upward, $\mathbf{\Omega}=\Omega\hat{\mathbf{e}}_z$ with $\Omega>0$, so that the rotation is clockwise when seen from below. The rotation of the fluid is set long before an experiment, in order to avoid transient spin-up recirculation flows and to achieve a solid body rotation regime. A cover is placed below the free surface at a distance $h=44$ cm from the bottom, defining a volume of working fluid of 54 l. This cover prevents surface waves and β effects due to the parabolic shape of the free surface.

Turbulence is generated by rapidly towing a corotating square grid at constant velocity V_g from the bottom to the top of the tank. During the subsequent decay of turbulence, the

TABLE I. Summary of experimental conditions. Ω is the turntable angular velocity, V_g the maximum grid velocity at midheight, $\mathrm{Re}_g = V_g M/\nu$ and $\mathrm{Ro}_g = V_g/2\Omega M$ the initial Reynolds and Rossby numbers based on the grid velocity and the mesh size, $M = 39$ mm. $\Omega t_E = h(\Omega/\nu)^{1/2}$ is the nondimensional Ekman time.

Symbol	Ω (rad s^{-1})	V_g (m s^{-1})	Re_g	Ro_g	Ωt_E
*	0.13	1.17	4.7×10^4	120	140
◇	0.53	0.82	3.1×10^4	19	310
○	1.5	0.82	3.1×10^4	6.8	540
●	1.5	1.63	6.2×10^4	14	540
□	4.3	0.82	3.1×10^4	2.4	930

grid is kept fixed close to the top of the tank. The grid consists of 1-cm-square bars with a mesh $M = 39$ mm, and has a solidity ratio (solid to total area) of 0.45. It is rigidly attached at its center point to a stainless-steel shaft that passes through a hole in the cover. The vertical translation of the grid is achieved by a 5-kW servo-controlled brushless motor. Grid velocities from $V_g = 0.82$ to 1.63 m s^{-1} have been used for the present experiments (see Table I). The grid velocity is constant throughout the height of the tank, except for the case $V_g = 1.63$ m s^{-1}, for which the accelerations and decelerations phases near the bottom and the top of the tank restrict the range of constant velocity to approximately $0.3h$.

A number of grid-generated turbulence experiments in a wind tunnel are shown to produce nearly isotropic fluctuations for a downstream distance larger than about $20-40M$.[34] Although this idealized situation cannot be achieved in our closed geometry, for which the height of the tank is only of about $10M$, one may however expect the turbulent velocity field to be approximately isotropic for times $t > (20-40)M/V_g$ after the grid translation. After this time, the velocity fluctuations have decreased down to about $u' \simeq 0.05V_g$ (velocity measurements are described in Sec. II B), and the turbulence enters into an inertial decay regime. This regime longs for typically 40 s, which is approximately 1000 inertial time scales M/V_g, after which the flow undergoes its final period of decay, where the friction from the Ekman layers becomes dominant.

B. Velocity measurements

Instantaneous velocity fields in the horizontal plane (x,y) at midheight of the tank are obtained from particle image velocimetry (PIV).[35] The water is seeded by borosilicate spheres, 11 μm in diameter, and illuminated by a horizontal laser sheet of thickness $b \simeq 1$ mm, located at midheight $h/2$, produced by a double-pulsed Nd:YAG laser (25 mJ/pulse). The flow is imaged through the transparent bottom of the tank with a double-buffer high-resolution camera (1280×1024 pixels, 4096 gray levels), located 50 cm below the laser sheet and corotating with the tank. Only a central region of 16×13 cm^2 of the flow is imaged, where negligible wall effects are expected. For practical reasons, the laser source is kept in the laboratory frame. The laser sheet being invariant under rotation about the vertical axis, accurate tracking of the particles is possible between the two successive images, assuming a time separation much lower than the rotation period of the turntable.

A set of 100 image pairs are acquired during the decay of turbulence. Since the rms velocity decreases in time, the delay between the two successive images of a pair is made to gradually increase during the acquisition sequence, from about 1 to 100 ms, so that the typical particles displacement remains constant, of order of 5–10 pixels, during all the decay. It has been checked than the time delay between the images of a pair remains well below the small-scale turnover time $1/\omega'$ throughout the decay. A careful calibration of this delay is a critical requirement for accurate PIV computations of the velocity fields.

For the PIV computations, interrogation windows of size 16×16 pixels, with an overlap of 8 pixels, were used. The final velocity fields are defined on a 160×128 grid, with a resulting spatial resolution of 1 mm, which is close to the laser sheet thickness. This allows us to accurately resolve the inertial scales of the flow, but may fail to resolve the dissipative scales when the Reynolds number is very large, in the first period of the decay, for which the Kolmogorov scale can be as low as $\eta \simeq 0.2$ mm. Here $\eta = (\nu^3/\epsilon)^{1/4}$, where ν is the kinematic viscosity and ϵ the instantaneous energy dissipation rate. A velocity resolution of 0.1 pixel can be achieved using a classical subpixel interpolation scheme for the correlation function. The resulting velocity signal-to-noise ratio is about 2×10^{-2}, allowing us to compute power spectra with more than three decades in energy. A Gaussian filter is applied when spatial derivatives, such as vorticity (Sec. III) or longitudinal velocity derivative (Sec. V), are needed. The error on the spatial derivatives can be estimated to about 5% at moderate Reynolds numbers, and up to 10%–20% at larger Reynolds numbers due to the insufficiently resolved Kolmogorov scale.

Since each realization of the decay is highly fluctuating, convergence of the statistics is achieved by computing ensemble averages for the same time delay t after the grid translation over several independent realizations of the decay. About 50 decays are recorded for each flow parameters, with a delay of at least 3 min (typically $5000M/V_g$) between two grid translations. It is worth noting that true ensemble averages are usually not achievable in most turbulence experiments, which usually make use of spatial or temporal averages instead.

C. Nondimensional numbers

Three parameters are needed to fully characterize the flow states during the decay: the grid velocity V_g, the back-

ground angular velocity Ω, and the time delay after the grid translation, t. From the first two parameters, V_g and Ω, which specify the initial conditions, the grid Reynolds and Rossby numbers are defined, $\mathrm{Re}_g = MV_g/\nu$ and $\mathrm{Ro}_g = V_g/2\Omega M$, respectively. For the present experiments, Re_g lies in the range $3\times10^4 - 6\times10^4$ (see Table I), insuring a fully developed turbulence in the wake of the grid. The Rossby number Ro_g is relatively large even for high rotation rate, between 2.4 and 120, so that the turbulent energy production in the near wake of the grid is essentially unaffected by the rotation. As a consequence, the early stage of the turbulence decay is expected to be nearly isotropic, and the background rotation gradually affects the flow in the course of the decay. For the third parameter, the time delay t after the grid translation, two nondimensionalizations are of interest depending on which physical effect is being investigated. The nondimensional time based on the grid time scale, $\tau = tV_g/M$, is useful to compare the decay in the presence of rotation with that without rotation, while the nondimensional time based on the background rotation, $\Omega t = \tau/(2\mathrm{Ro}_g)$, is useful for situations dominated by the Coriolis force (e.g., for the buildup of the vorticity skewness, Sec. III B).

It may also be of interest to introduce the turbulent *macro* Reynolds and Rossby numbers, based on the instantaneous horizontal velocity rms $u' = \langle u_x^2 + u_y^2 \rangle^{1/2}/2$ and the mesh size M,

$$\mathrm{Re}_M = u'M/\nu, \quad \mathrm{Ro}_M = u'/2\Omega M \tag{1}$$

(the brackets $\langle\cdot\rangle$ denote spatial and ensemble average). These numbers are usually defined from the integral length scales,[8] which are increasing functions of time in decaying turbulence, starting from values of order of the mesh size M at early times. However, our measurements being restricted to a central rectangular area of size $4.0M \times 3.2M$, the large scale limit of the velocity correlation function could not be accurately defined, and we had to make use of macro Reynolds and Rossby numbers based on the mesh size M instead, which systematically underestimate the actual ones. As the turbulence decays, both Re_M and Ro_M decrease in time, with the ratio $\mathrm{Ro}_M/\mathrm{Re}_M$ remaining constant. This ratio only depends on the angular velocity of the turntable and is given by $\mathrm{Ro}_g/\mathrm{Re}_g = (h/M)^2\mathrm{Ek}$, where $\mathrm{Ek} = \nu/2\Omega h^2$ is the Ekman number based on the tank height h, which lies in the range $3\times10^{-5} - 6\times10^{-7}$ for the present experiments.

Finally, since large Reynolds number turbulence gives rise to vorticity levels much larger than the inverse turnover time u'/M, small scales may escape from the influence of the background rotation even for large Ω. It is therefore of interest to introduce a *micro*-Rossby number,

$$\mathrm{Ro}_\omega = \omega'/2\Omega,$$

where $\omega' = \langle \omega_z^2 \rangle^{1/2}$ is the instantaneous rms of the vertical vorticity, that compares the small scale vorticity to the background vorticity. The error on ω' from the PIV measurement leads to an uncertainty of about 10%–20% on Ro_ω. The difference between the micro- and macro-Rossby numbers may vanish for asymptotically large rotation rates, for which the vorticity may become a large-scale quantity. However, for sufficiently large Reynolds numbers and moderate rotation rates, an intermediate range may exist, for which $\mathrm{Ro}_M \ll 1$ and $\mathrm{Ro}_\omega \gg 1$ simultaneously. In that range, the large scales are expected to be affected by the rotation whereas the small scales are not.[8] It is in that intermediate range that we are mainly interested, for which interactions between turbulence and inertial waves leads to a nontrivial dynamics, with possible energy transfers towards the 2D mode.

III. CYCLONIC/ANTICYCLONIC ASYMMETRY

A. Vorticity distributions

Figure 2 shows four snapshots of the vertical component of the vorticity fields, $\omega_z = \partial u_y/\partial x - \partial u_x/\partial y$, taken at four times during the decay, for $\Omega = 1.5$ rad s^{-1} and $V_g = 1.63$ m s^{-1} (data set ● in Table I). Each field is normalized by its instantaneous vorticity rms ω'. Since the pictures are taken from below, the system rotation is clockwise, so that cyclonic vorticity (in red) is associated with clockwise rotation and anticyclonic vorticity (in blue) with anticlockwise rotation.

Just after the grid translation, $\tau = tV_g/M \simeq 20$ [Fig. 2(a)], the vorticity field shows nearly symmetric small-scale disordered fluctuations. As time proceeds [$\tau \simeq 660$ and 1400, Fig. 2(b) and 2(c)], intense large-scale coherent vortices gradually appear, as the result of the increasing influence of the background rotation. These coherent vortices are essentially cyclonic (their vorticity is of the same sign than the background vorticity), as classically observed from experiments[5,6,31] and numerical simulations.[13,18] Anticyclonic vorticity is also present, but it is much weaker and does not show vortices as coherent as for cyclonic vorticity. Vortex sheets of moderate vorticity, of either cyclonic or anticyclonic sign, can be seen, surrounding the vortices and strained in the horizontal direction. These strained shear layers are visually similar to the filamentation of vorticity observed in the enstrophy cascade of 2D turbulence.[20] The prevalence of corotating cyclonic vortices probably enhances the horizontal straining of these shear layers, compared to the case of usual 2D turbulence, where vortices of both positive and negative signs are present. In the neighborhood of the intense cyclones, vortex sheets spiraling in the clockwise direction are frequently encountered, indicating the presence of axial stretching in the core of the vortices. For the last image, $\tau \simeq 2800$ [Fig. 2(d)], only a strong cylonic vortex with nearly circular cross section, surrounded by a weak turbulent background, is present in the field. Expressed in units of the rotation time scale, the corresponding time is $\Omega t \simeq 100$ in this case. As will be shown in Sec. III B, the effect of the Ekman friction is dominant at that time, and the last isolated cyclonic vortices are eventually damped by Ekman friction.

The asymmetry between cyclonic and anticyclonic vorticity clearly appears from the vorticity distributions shown in Fig. 3, taken at three times during the decay. The same probability density functions (pdf), $p(\omega_z)$, are shown normalized either by the background vorticity 2Ω [Fig. 3(a)] or by the instantaneous vorticity rms ω' [Fig. 3(b)]. Just after the grid translation, $p(\omega_z)$ is nearly symmetric, but as time evolves it becomes strongly positively skewed, confirming

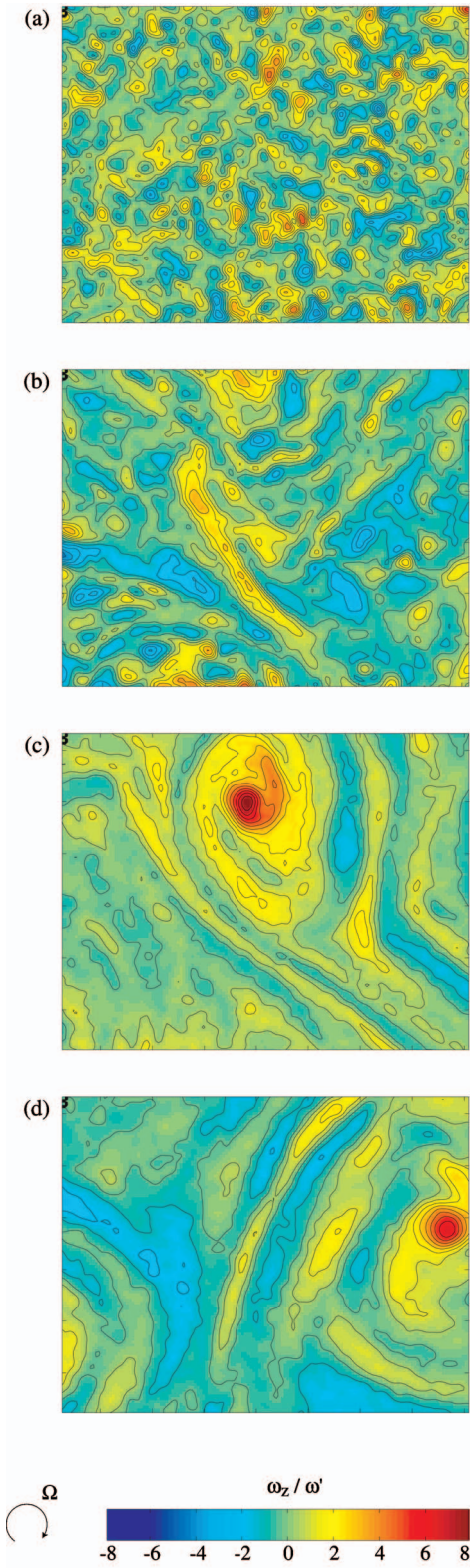

FIG. 2. (Color). Normalized vertical vorticity fields ω_z/ω' at four successive times for $\Omega=1.5$ rad s^{-1} and $V_g=1.63$ m s^{-1} (data set ● in Table I). The imaged rectangle represents 16 cm×13 cm, i.e., about 17% of the section of tank. Twenty-two equally spaced contour levels are shown in the range $[-8\omega', 8\omega']$. (a) $(\tau, \mathrm{Re}_M, \mathrm{Ro}_\omega) \simeq (20, 4400, 6.4)$. (b) (660, 855, 0.61). (c) (1400, 520, 0.27). (d) (2800, 210, 0.11).

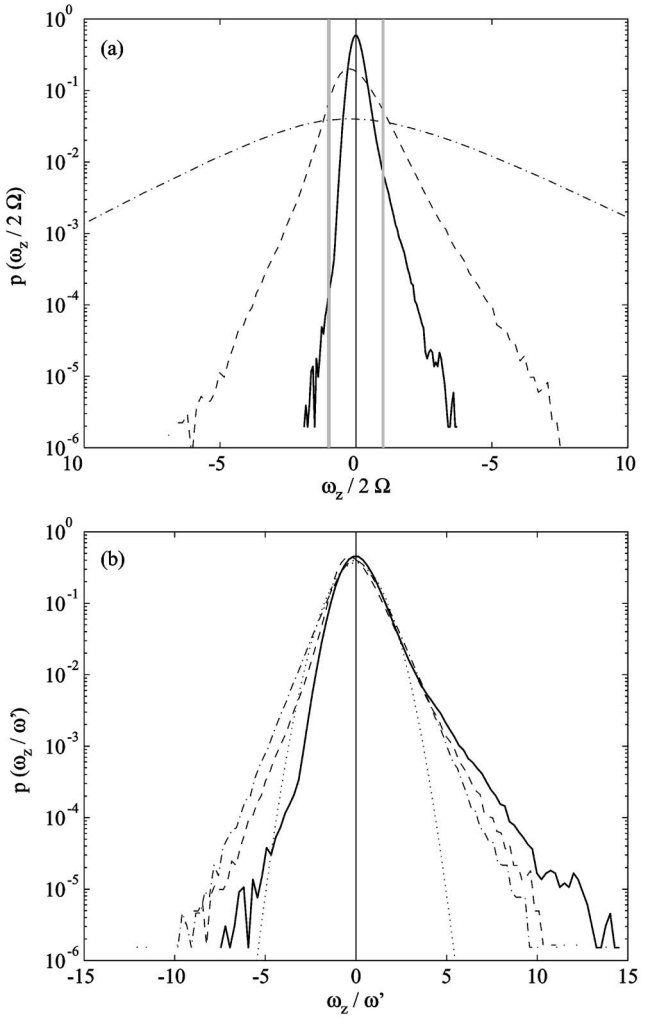

FIG. 3. Probability density function of the axial vorticity ω_z at three times during the decay, for $\Omega=1.5$ rad s^{-1} and $V_g=0.82$ m s^{-1} (data set ○ in Table I), (a) normalized by the background vorticity 2Ω; (b) normalized by the instantaneous vorticity rms ω'. - · -, $(\tau, \mathrm{Re}_M, \mathrm{Ro}_\omega)=(20, 1990, 3.9)$; - - , (230, 780, 0.8); —, (660, 440, 0.26). In (a), the vertical gray lines indicate $\omega_z=\pm 2\Omega$. In (b), the dotted curve shows a Gaussian distribution.

the visual evidence of the cyclonic vorticity prevalence. For $\tau \simeq 230$, the pdf shows an approximately exponential tail for $\omega_z > 3\omega'$, while the negative vorticity fluctuations show a slightly sub-Gaussian distribution. It may be noted that this asymmetry is more pronounced when the extreme fluctuations are of the order of the background vorticity 2Ω [indicated by the vertical gray lines in Fig. 3(a)], i.e., when the associated micro-Rossby number $\omega_z/2\Omega$ is of order of 1. For this pdf, the cyclonic versus anticyclonic probability ratio taken at $|\omega_z|=2\Omega$, $p(2\Omega)/p(-2\Omega)$, is of order of 100.

The prevalence towards cyclonic vorticity is a generic feature of rotating systems, which has received a number of experimental and theoretical characterizations.[10–12,36,37] Two mechanisms may explain this asymmetry. First, since the vortex stretching and tilting by the turbulent strain act on the absolute vorticity $\boldsymbol{\omega}+2\Omega\hat{\mathbf{e}}_z$, vorticity with a positive component along $\hat{\mathbf{e}}_z$, i.e., cyclonic vorticity, is more amplified in average. Shear layers of cyclonic vorticity are thus more likely to be strengthened and to roll up into cyclonic vortices, while those of anticyclonic vorticity remain weak and are destabilized by the surrounding turbulence. This amplification mechanism is essentially present at the early time of the decay, for a moderate Rossby number, since for longer times

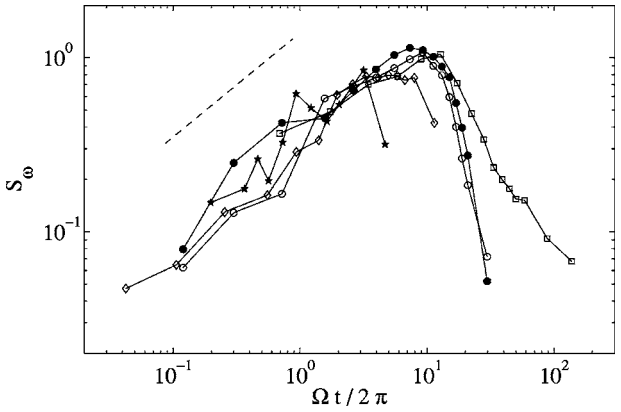

FIG. 4. Vorticity skewness S_ω as a function of the number of tank rotation $\Omega t/2\pi$, for the five data sets (see the symbols in Table I). The dashed line shows a power law $(\Omega t)^{0.6}$.

the flow may become quasi-2D and the vertical strain should consequently become much weaker. The second reason for the cyclonic vorticity prevalence is an inertial instability modified by the Coriolis force, which leads to a selective destabilization of the anticyclonic regions.[11] For idealized axisymmetric vortices, this instability may be described in terms of a generalized Rayleigh criterion,[36,37] which includes the effect of the background rotation. This criterion predicts that cyclonic regions are stabilized by the background rotation, while anticyclonic regions of negative absolute vorticity, i.e., having $\omega_z < -2\Omega$, may be unstable with respect to axisymmetric disturbances. This is consistent with the pdfs of Fig. 3(a), which show a maximum asymmetry when the tails are of order of the background vorticity 2Ω.

B. Vorticity skewness

A useful quantity to further quantify the prevalence towards cyclonic vorticity as time evolves is the vorticity skewness factor, first introduced by Bartello *et al.*,[13]

$$S_\omega = \frac{\langle \omega_z^3 \rangle}{\langle \omega_z^2 \rangle^{3/2}},$$

where the brackets $\langle \cdot \rangle$ denote spatial and ensemble average. S_ω is zero for symmetric vorticity fluctuations. A generic behavior for the buildup of S_ω in decaying rotating turbulence should only be expected if the decay starts from an initial homogeneous 3D turbulence, i.e., for large initial Reynolds and Rossby numbers, which is the case for the present experiment.

The time histories for S_ω are shown in Fig. 4 as a function of the number of tank rotations $\Omega t/2\pi$. The curves for the different data sets follow the same trend for approximately the first five rotations, showing an approximate power law

$$S_\omega \sim (\Omega t)^{0.6 \pm 0.1}. \tag{2}$$

Using Ωt as the nondimensional time shows no significant influence of V_g and Ω in that range, indicating that Ω^{-1} is the relevant time scale for the buildup of the vorticity asymmetry. This observation suggests that this growing asymmetry is supported by inertial waves, of maximum frequency given by 2Ω. From heuristic statistical arguments, Gence and Frick[39] indeed showed that the time scale for the buildup of the vorticity triple correlation in rotating homogeneous turbulence is Ω^{-1}. However, the power-law behavior (2) observed here is a long-time nonlinear effect, which cannot be inferred from their short-time analysis.

At larger times, S_ω saturates to a value $\simeq O(1)$, and then sharply decreases, at a time t_c that depends on Ω. This decay probably results from the effect of the confinement. As the characteristic length of the coherent cyclonic vortices reaches the height of the tank, h, the Ekman layers on the top and bottom walls induce a vertical pumping of the fluid, from the boundary layers into the core of the vortices for the cyclonic vorticity and inversely for the anticyclonic vorticity.[1,9] In the case of the cyclonic vortices, which are more abundant, this Ekman pumping induces a vortex compression that weakens the circulation of the vortices, on a time scale given by $t_E = h(\nu\Omega)^{-1/2}$, which represents the characteristic time for a fluid particle to travel along the tank height at the vertical velocity of this secondary flow. Although the moderate range for Ω does not allow to accurately verify the scaling of this time scale, the times t_c for which S_ω is maximum are found to be

$$t_c \simeq (0.10 \pm 0.02) h(\nu\Omega)^{-1/2} \tag{3}$$

[the values for the Ekman time scale $t_E = h(\nu\Omega)^{-1/2}$ are given in Table I], indicating that the confinement is indeed responsible for the decrease of S_ω for $t > t_c$. It must be noted that the instantaneous Reynolds number Re_M for the different data sets is not constant at that time t_c, taking values ranging from 350 to 850, ruling out a possible low Reynolds number effect for the decrease of S_ω at $t > t_c$. The two curves for the data sets at $\Omega = 1.5$ rad s^{-1} (symbols ○ and ● in Table I) approximately coincide, confirming that V_g has no direct influence on the maximum of S_ω (provided that Re_M remains sufficiently large at $t \simeq t_c$).

Although the above argument correctly explains the cutoff (3) for the growth of the vorticity skewness, it must be noted however that the *decrease* of S_ω for $t > t_c$ cannot be explained within the classical linear Ekman theory. A purely linear Ekman pumping, which is valid only for $\mathrm{Ro}_\omega \ll 1$, should equally affect the cyclonic and the anticyclonic vorticity,[1] leading to exponentially decreasing vorticity of both sign, and should therefore let S_ω unchanged. On the other hand, if the limit $\mathrm{Ro}_\omega \ll 1$ does not hold, as is the case in our experiment ($\mathrm{Ro}_\omega = 0.1 - 0.4$ for $t \simeq t_c$), nonlinear corrections to the Ekman pumping should be considered, which are shown to enhance the damping of the cyclonic vortices (e.g., Zavala Sansón and van Heijst[38]). As a result, a gradual resymmetrization of the vorticity distribution should be expected on a time scale $O(t_E)$, and may explain the observed decay of S_ω. Accordingly, the self-similar growth (3) may be considered as a generic feature of decaying rotating turbulence, while the maximum of S_ω is constrained by the finite size effects.

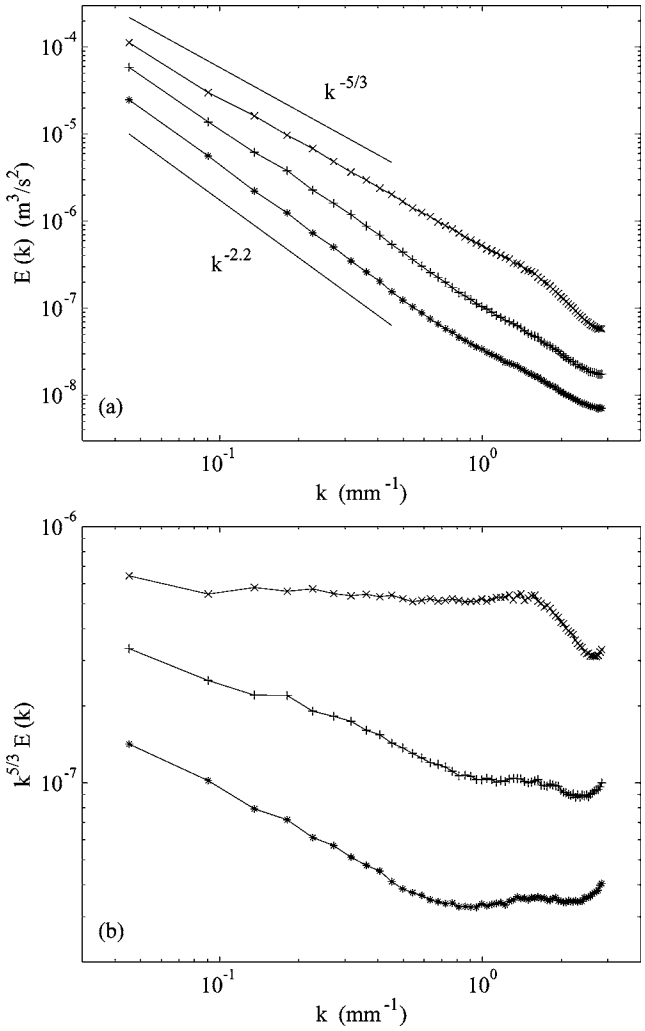

FIG. 5. (a) Energy spectra for different Rossby numbers at three times during the decay, for $\Omega=1.5$ rad s^{-1} and $V_g=1.63$ m s^{-1} (data set ● in Table I). ×, $(\tau,\mathrm{Re}_M,\mathrm{Ro}_\omega)=(50,3400,5.5)$; +, (230, 1200, 1.2); *, (700, 600, 0.35). (b) Same spectra compensated by $k^{5/3}$.

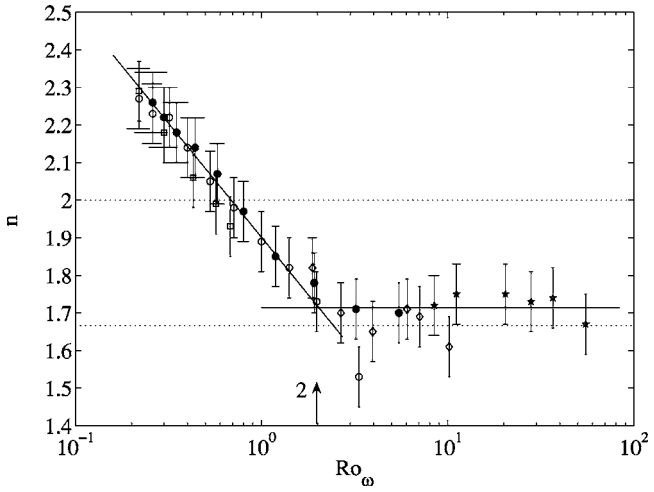

FIG. 6. Exponent n of the power spectrum as a function of the instantaneous micro-Rossby number Ro_ω, for the five data sets (see the symbols in Table I). Time proceeds from large to small Ro_ω. The lower dotted line corresponds to the exponent 5/3 of the Kolmogorov spectrum, and the upper one shows the exponent 2 (see the text). The solid lines are guide for the eye.

IV. ENERGY SPECTRUM

We now turn to the influence of the background rotation on the scaling of the energy spectrum. The 1D energy spectrum $E(k)$, where k is the horizontal wave number, is computed from the 2D Fourier transform of the velocity field truncated to a central 13×13 cm^2 square, and ensemble averaged over 50 statistically independent realizations at a fixed delay t after the grid translation.

Figure 5(a) shows three energy spectra, obtained at three times during the decay. Just after the grid translation, for $\tau=50$, the energy spectrum shows a well-defined scaling range over more than one decade, with a power law close to $k^{-5/3}$, as expected for 3D isotropic turbulence without significant rotation effect. It must be noted that the power laws extend to wave numbers significantly smaller than the forcing wave number $k_f=2\pi/M\simeq0.16$ mm^{-1} (where M is the mesh size), at which energy is initially injected. This generic feature of decaying turbulence, even in the absence of rotation, is related to the increase of the integral length scale, and does not necessarily imply the existence of a net inverse energy cascade at low wave numbers. No resolved dissipative range can be seen for large wave numbers, due to the limited resolution of the PIV. The spectral behavior of the PIV noise for large wave numbers is possibly due to nontrivial biases in the computation of the image correlations,[40] and we therefore focus on small wave numbers, $k<1$ mm^{-1}. Later on, for $\tau=230$ and 700, an inertial range is still present, but the power law becomes steeper, with a slope that gradually increases as time proceeds, reflecting the growing importance of the large scales compared to the small ones. This may be further seen in Fig. 5(b), showing the same three spectra compensated by $k^{5/3}$. While a well-defined plateau is observed at short time, about one decade of power laws with negative slopes is obtained for $\tau=230$ and 700. For even larger times, no clear scaling can be defined from the energy spectrum over a reasonable range of wave numbers, and exponents larger than 2.3 are not found. This lack of scaling occurs for times that approach the Ekman cutoff (3), i.e., it probably results from a confinement effect.

The spectral exponent n is shown for the five data sets in Fig. 6. This exponent is determined by plotting the compensated spectrum $k^nE(k)$ and adjusting the value of n in order to obtain a well-defined plateau for the first decade of wave numbers. An error bar for n can be estimated from this procedure, of about 0.1, as the acceptable range for which a plateau may be defined. Although the scatter is important, a clear trend for n appears when plotted as a function of the instantaneous micro-Rossby number Ro_ω. For large Ro_ω, n takes values $\simeq1.7\pm0.1$, close to the expected 5/3 for the Kolmogorov spectrum in the absence of rotation. This slight systematic departure from 5/3 is indeed a well-known intermittency effect, and values close to 1.7 are classically obtained in other experimental configurations.[41] As Ro_ω decreases in time, n is found to gradually increase from 1.7 up to 2.3 ± 0.1, with a crossover that takes place at $\mathrm{Ro}_\omega\simeq2\pm0.5$. At the location of this crossover, the Ekman layers

effects are not present yet, and the Reynolds number covers a significant range, from 200 to 2000, so that the steepening of the spectral slope is presumably a true effect of the background rotation. Moreover, the macro-Rossby number Ro_M lies in the range 0.2–0.7 at the crossover, confirming that the micro-Rossby number Ro_ω is the most relevant instantaneous control parameter that governs the scaling of the energy spectrum (plotting the slope n as a function of Ro_M would increase the horizontal scatter by a factor of 3). This conclusion is actually not straightforward, since the effects of the rotation may be first expected at large scales, and should therefore be governed by the macro-Rossby number Ro_M, with a gradual steepening of the energy spectrum at low wave numbers. However, a Ro_M dependence of the spectral slope cannot be totally ruled out from the present experiment, because of the restricted range for which $\mathrm{Ro}_\omega > 1$ and $\mathrm{Ro}_M < 1$ simultaneously.

It is worth pointing out that a k^{-2} regime is not supported by our data, except as a transient state for $\mathrm{Ro}_\omega \simeq 0.5$. Spectrum $E(k) \simeq k^{-2}$ for rotating turbulence was predicted by Zhou[21] and Canuto and Dubovikov[22] on phenomenological grounds, assuming that the time scale for energy transfers is given by the rotation time scale Ω^{-1} instead of the classical nonlinear time scale, but without explicitly taking account of the anisotropy of the flow. In their analysis, the k^{-2} spectrum is limited to low wave numbers, $k \ll \Omega^{3/2}\epsilon^{-1/2}$, for which the *local* Rossby number is $\ll 1$, whereas the classical $k^{-5/3}$ is recovered for larger wave numbers. Although some evidence of a k^{-2} law can be found in experiments[25] and simulations,[23,24] it may be an effect of a moderate Rossby number, for which the anisotropy is indeed weak. This conclusion agrees with the recent LES results of Yang and Domaradski,[29] who do observe a k^{-2} as a transient state for moderate Rossby number as well, but a steeper spectrum for smaller Rossby numbers.

An asymptotic analysis, in the limit of quasi-infinite Reynolds number and quasizero Rossby number, has been recently carried out using the formalism of wave turbulence theory by Galtier,[26] leading to a 3D anisotropic spectrum $e(\mathbf{k}) \sim k_\parallel^{-1/2} k_\perp^{-7/2}$, where $k_\parallel$ and $k_\perp$ are the wave-number components along the rotation axis and normal to it, respectively. In a similar approach, starting from a generalized eddy-damped quasinormal Markovian (EDQNM) model, Cambon, Rubinstein, and Godeferd[27] derived a 3D spectrum $e(\mathbf{k}) \sim k_0^{-1/2} k_\parallel^{-1/2} k_\perp^{-3}$, where k_0 is a cutoff in the horizontal plane. Numerical integration of this model[30] yields a $E(k) \simeq k^{-3}$ form for the one-dimensional (1D) spherically averaged spectrum, this scaling being the result of a combination of a k^{-2} scaling for nearly horizonal wave numbers and a steeper scaling for nearly vertical ones. Although direct comparison between these predictions and our spectra is not straightforward, because only two components of the velocity in the plane normal to the rotation axis are experimentally measurable, these two predictions are expected to give 1D spectra steeper than k^{-2}, which is consistent with our observations.

V. ENERGY TRANSFERS

A. Velocity increments skewness

Further insight into the steepening of the energy spectrum for $\mathrm{Ro}_\omega < 2$ may be obtained by inspecting the influence of the background rotation on the energy transfers in physical space. Using the assumption of isotropy, the scale-to-scale energy transfers may be characterized by the statistics of the longitudinal velocity increment $\delta_r u = [\mathbf{u}(\mathbf{x}+\mathbf{r}) - \mathbf{u}(\mathbf{x})] \cdot \mathbf{r}/r$ across the separation $r = |\mathbf{r}|$. The second-order moment of this quantity, $\langle \delta_r u^2 \rangle$, is a measure of the kinetic energy at scale r, while the third-order moment, $\langle \delta_r u^3 \rangle$, is related to the mean energy flux at that scale. In particular, the sign of $\langle \delta_r u^3 \rangle$ gives the direction of the energy flux through that scale: positive for transfers towards larger scales, and negative for transfers towards smaller scales.

For high-Reynolds number nonrotating isotropic turbulence, energy is transferred at a constant rate for all scales in the inertial range, and $\langle \delta_r u^3 \rangle$ satisfies Kolmogorov's 4/5th law:[41]

$$\langle \delta_r u^3 \rangle = -\tfrac{4}{5}\epsilon r, \tag{4}$$

where ϵ is the mean energy dissipation. The energy proceeds, in average, from large to small scales. This law still applies for decaying turbulence, where ϵ must be interpreted as the instantaneous energy dissipation rate.[42] This relation indicates that longitudinal velocity increments are negatively skewed, i.e., compressive strain is less likely but more intense than extensional strain.[3] For strictly 2D turbulence, one has to distinguish between the two possible cascade regimes. For r larger than the injection scale, in the inverse energy cascade, the transfers proceed from small to large scale, and $\langle \delta_r u^3 \rangle$ is positive.[20] On the other hand, for r smaller than the injection scale, in the enstrophy cascade, there is no energy transfer and $\langle \delta_r u^3 \rangle$ should be zero.[43]

In Fig. 7(a) is plotted $\langle \delta_r u^3 \rangle$ as a function of r, where $\delta_r u$ denotes here the longitudinal velocity increments in the plane normal to the rotation axis, at three times during the decay, for $\Omega = 1.5$ rad s^{-1} and $V_g = 1.63$ m s^{-1} (data set ● in Table I). At early time, $\tau \simeq 80$, $\langle \delta_r u^3 \rangle$ is negative for all r and approximately proportional to r for 1.5 cm $< r <$ 6 cm, in agreement with the 4/5th law (4) for the nonrotating case. This behavior holds for scales slightly larger than the mesh size, $M = 3.9$ cm, which is consistent with the scaling range on the energy spectrum that begins for $k < 2\pi/M$. As time proceeds, the magnitude of $\langle \delta_r u^3 \rangle$ strongly decreases, essentially due to the decay of the energy dissipation rate ϵ. While $\langle \delta_r u^3 \rangle$ remains negative at small scales, its sign changes for $r \simeq 1-2$ cm and becomes positive for larger r, suggesting that a net inverse energy cascade begins to develop at large scales. Similar observations were reported by Simand *et al.*[44] from one-point measurements in the vicinity of a strong localized vortex. The scale at which the flux vanishes is found to decrease in time, in agreement with the expected picture of a direct energy cascade confined to smaller scales as the influence of the rotation increases. However, since no energy supply is present, this double cascade regime can only take place as a transient state during the decay.

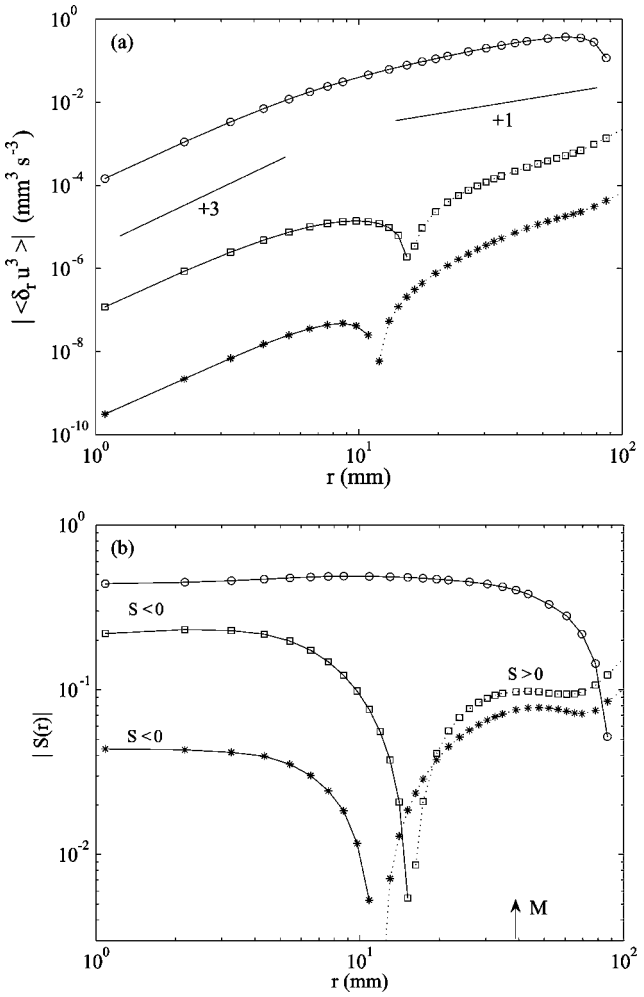

FIG. 7. (a) Third-order moment of the longitudinal velocity increments as a function of the scale r, at three different times during the decay. Negative values are plotted with full lines, and positive values with dotted lines. (b) Skewness of the longitudinal velocity increments (5). ○, $\tau=80$; □, $\tau=820$; *, $\tau=2200$.

Since the energy dissipation rate ϵ decreases in time during the decay, at a rate that may moreover depend on the Rossby number, it is convenient to normalize $\langle \delta_r u^3 \rangle$ by introducing the skewness of the velocity increments

$$S(r) = \frac{\langle \delta_r u^3 \rangle}{\langle \delta_r u^2 \rangle^{3/2}} \tag{5}$$

to characterize the instantaneous relative energy transfers. Assuming normal scaling (i.e., neglecting intermittency effects), one has $\langle \delta_r u^2 \rangle \sim (\epsilon r)^{2/3}$, so that the skewness factor $S(r)$ should be independent of r for inertial scales. The direction of the energy cascade may be then solely described by the sign of the skewness: $S(r)<0$ for the direct cascade, $S(r)>0$ for the inverse cascade, and $S(r)=0$ in the absence of energy transfers.

The skewness of the velocity increments, $S(r)$, is plotted in Fig. 7(b) for the same data set as in Fig. 7(a). It must be noted that computing $S(r)$ from PIV measurements is a delicate issue, as very large statistics are needed to ensure a correct convergence of odd moments. Assuming a symmetrically distributed PIV noise, a bias is introduced towards small values of $|S(r)|$, which may be significant at small scales. A smoothing procedure using a Gaussian filter is applied to the velocity fields in order to minimize this effect. The size of the smoothing windows is carefully chosen as the smallest size leading to a nondecreasing $|S(r)|$ as $r \to 0$. No bias is expected from this procedure, since in 3D turbulence $|S(r)|$ should monotonically increase as $r \to 0$. Filter sizes between 1 and 1.5 collocation points have been used for the three curves in Figs. 7(a) and 7(b). This procedure is expected to give reliable results for moderate Reynolds numbers, for which the Kolmogorov scale η is slightly smaller or of the same order of the spatial resolution, but may significantly underestimate the actual skewness for larger Reynolds numbers. The relative error can be estimated to about 20% for small r when averaging over 50 statistically independent velocity fields, but may be even larger for separations r comparable to the image size, for which poor statistics is available.

At early time $S(r)$ is approximately constant for scales $r<6$ cm, taking values around -0.45 ± 0.03. Values in the range 0.4–0.5 are typical for nonrotating experiments and simulations.[41] As time proceeds, the magnitude of $|S(r)|$ decreases at small scales, a clear indication of the inhibition of the energy transfers by the background rotation. For the second and third curves, the Reynolds number Re_M is 750 and 320, respectively, values for which $S(r) \simeq -0.4$ in the nonrotating case, confirming that the decrease of $|S(r)|$ is not a weak Reynolds number effect but a true effect of the rotation. The positive skewness at larger scales, in the inverse energy cascade, is weak, $S(r) \simeq 0.06-0.10$, a value in qualitative agreement with numerical simulations of strictly 2D forced turbulence.[45]

B. Velocity derivative skewness

In order to further characterize the influence of the Reynolds and Rossby numbers on the energy transfers, we finally focus on the longitudinal velocity derivative skewness,

$$S = \frac{\langle (\partial u/\partial r)^3 \rangle}{\langle (\partial u/\partial r)^2 \rangle^{3/2}}, \tag{6}$$

which is approximated by taking $r \to 0$ in Eq. (5). This quantity is of first interest, since it is directly related to the enstrophy production.[2,3] Direct cascade of energy in 3D turbulence is associated to a positive enstrophy production, and hence to a negative velocity derivative skewness. On the other hand, no enstrophy production is present in 2D turbulence, and S is zero (this result follows from a purely kinematical constraint, since incompressibility requires that the two normal strain rates are opposite and of equal magnitude for a 2D flow). In rotating 3D turbulence, the scrambling effect of inertial waves leads to a damping of the velocity derivative skewness,[16] so that $|S| \to 0$ just reflects the inhibition of the energy transfers but is not a sufficient condition for a 2D state.

The skewness of the velocity derivative is plotted as a function of the instantaneous micro-Rossby number in Fig. 8, for the five different data sets in Table I. All the measured skewness are found negative. As previously mentioned, the

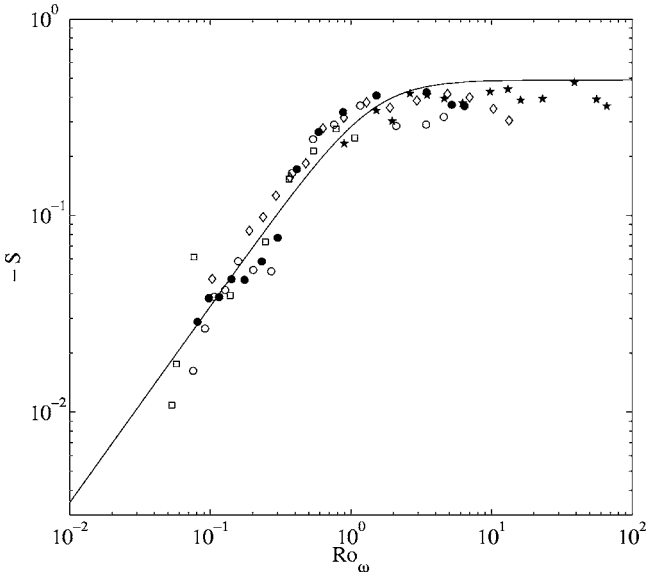

FIG. 8. Skewness of the longitudinal velocity derivative (6) as a function of the instantaneous micro-Rossby number Ro_ω, for the five data sets (see symbols in Table I). Time proceeds from large to small Ro_ω. The line is the model equation (7) from Cambon *et al.* (Ref. 16).

error bar is of about 20%, a value which is consistent with the scatter of the different data sets. For large Ro_ω, S is approximately constant, $S \simeq -0.40 \pm 0.05$, while for smaller Ro_ω it decreases approximately as $|S| \propto \mathrm{Ro}_\omega$. The crossover between these two regimes, $\mathrm{Ro}_\omega \simeq 1-2$, remarkably coincide with the crossover found for the spectral slope n (Fig. 6). As previously mentioned, at this crossover, Re_M is in the range 200–2000, ruling out a possible Reynolds number effect on the transition. These observations indicate that the energy spectrum starts departing from the Kolmogorov form $k^{-5/3}$ at the point where the background rotation starts inhibiting the energy transfers. This is a nontrivial result, since S is a small-scale quantity, while the spectral exponent n describes the full inertial range.

The experimental data are found to compare well with the model equation

$$S = \frac{-0.49}{(1 + 2\mathrm{Ro}_\omega^{-2})^{1/2}}, \tag{7}$$

proposed by Cambon *et al.*[16] to fit earlier DNS results, which is also shown in Fig. 8. In their analysis, the denominator was suggested from the isotropic EDQNM closure,[46] where the effect of the rotation was taken into account by simply replacing in the eddy-damped coefficient the nonlinear time scale estimated from the enstrophy, $\langle \omega^2 \rangle^{-1/2}$, by the one from the absolute enstrophy, $[\langle \omega^2 \rangle + (2\Omega)^2]^{-1/2}$. The value -0.49 for $\mathrm{Ro}_\omega \gg 1$ was borrowed from the infinite Reynolds isotropic EDQNM model without rotation.[46] A slightly lower magnitude for $|S|$ at large Ro_ω is measured experimentally, $|S| \simeq 0.40 \pm 0.05$ instead of 0.49, probably due to the insufficiently resolved small scales from the PIV computations, which are more pronounced at large Reynolds number. A model similar to (7) was also derived by Park and Chung,[47] on the basis of the k^{-2} spectrum proposed by Zhou.[21] Although anisotropy effects are ignored in both approaches, these crude models remarkably capture the behavior of the experimental data. This agreement with isotropic models indicates that the damping of the velocity derivative skewness at small Ro_ω is not directly related to the two-dimensionalization process, but just reflects the inhibition of the energy transfers originating from the scrambling effect of the inertial waves.

VI. DISCUSSION AND CONCLUSION

A series of grid-generated turbulence experiments in a rotating frame has been carried out, with the aim of investigating the influence of the background rotation on the turbulence decay starting from approximately homogeneous and isotropic initial conditions (large initial Reynolds and Rossby numbers). Three quantities have been systematically characterized in the course of the decay: the vorticity skewness, which traces the asymmetry between the cyclonic and anticyclonic vorticity, the spectral slope of the energy spectrum, and the skewness of the velocity derivative, which characterizes the scale-to-scale energy transfers in physical space.

Starting from approximately homogeneous 3D turbulence with symmetric vorticity fluctuations, an asymmetry towards cyclonic vorticity gradually builds up, with a growth of the vorticity skewness as $S_\omega \sim (\Omega t)^{0.6 \pm 0.1}$, up to values $O(1)$. This growth is interrupted for times $t_c \simeq 0.1 h (\nu\Omega)^{-1/2}$ (typically three to ten tank rotations), for which nonlinear Ekman friction on the top and bottom walls preferentially reduces the cyclonic vorticity.[38] As a consequence, the observed maximum of S_ω probably results from finite size effects, and larger values should be observable in larger experiments, for which the Ekman friction effects should be delayed.

Although the background rotation is shown to have a deep influence on the vorticity asymmetry from the early time, it has been shown to have no significant effect on the spectrum and the energy transfers as long as the instantaneous micro-Rossby number remains sufficiently large. The slope of the energy spectrum and the velocity derivative skewness are found to remain close to their classical values for $\mathrm{Ro}_\omega > 2 \pm 0.5$ ($n \simeq 5/3$ and $S \simeq -0.4$), as for nonrotating turbulence. On the other hand, as Ro_ω decreases below 2, the energy spectrum becomes steeper, and the magnitude of the velocity derivative skewness starts decreasing as $|S| \propto \mathrm{Ro}_\omega$, which is a clear signature of the inhibition of the energy transfers by the background rotation. This transition takes place at a time long before the Ekman friction time, $t < t_c$, suggesting that the observed behaviors of $E(k)$ and S are generic features of homogeneous decaying rotating turbulence.

Finally, it was noted that, in the range of Reynolds and Rossby numbers spanned by the present experiment, no saturation of the spectral exponent n could be observed as $\mathrm{Ro}_\omega \to 0$. Although the observed trend is not inconsistent with the limit $n \to 3$ that may be expected for turbulence dominated by rotation, this limit is very far from what can be achieved in our system. Crude extrapolation of the trend for n in Fig. 6 would lead to a k^{-3} spectrum for $\mathrm{Ro}_\omega < 10^{-2}$. Reaching such a small value while keeping an acceptable Reynolds

number would require rotation rates of about $\Omega \simeq 150$ rad s^{-1}, or equivalently dimensions larger by a factor of 5, which is obviously well beyond our experimental setup. One may conclude that using 3D isotropic turbulence as an initial condition in a decaying rotating experiment may hardly allow to observe a k^{-3} spectrum in a laboratory-sized experiment. Of course, this conclusion does not hold for inhomogeneous turbulence or nonisotropic forcing, which may lead to a k^{-3} spectrum at more reasonable Rossby numbers.

ACKNOWLEDGMENTS

We acknowledge C. Cambon and S. Galtier for fruitful discussions, and A. Aubertin, H. Auradou, G. Chauvin, and R. Pidoux for experimental help. We are indebted to A. Stegner for providing the rotating turntable apparatus.

[1] H. Greenspan, *The Theory of Rotating Fluids* (Cambridge University Press, Cambridge, 1968); J. Pedlosky, *Geophysical Fluid Dynamics* (Springer, New York, 1987).
[2] M. Lesieur, *Turbulence in Fluids* (Kluwer Academic, Dordrecht, 1997).
[3] P. A. Davidson, *Turbulence* (Oxford University Press, New York, 2004).
[4] A. Ibbetson and D. Tritton, "Experiments on turbulence in a rotating fluid," J. Fluid Mech. **68**, 639 (1975).
[5] A. D. McEwan, "Angular momentum diffusion and the initiation of cyclones," Nature **260**, 126 (1976).
[6] E. J. Hopfinger, F. K. Browand, and Y. Gagne, "Turbulence and waves in a rotating tank," J. Fluid Mech. **125**, 505 (1982).
[7] S. C. Dickinson and R. R. Long, "Oscillating-grid turbulence including effects of rotation," J. Fluid Mech. **126**, 313 (1984).
[8] L. Jacquin, O. Leuchter, C. Cambon, and J. Mathieu, "Homogeneous turbulence in the presence of rotation," J. Fluid Mech. **220**, 1 (1990).
[9] F. S. Godeferd and L. Lollini, "Direct numerical simulations of turbulence with confinement and rotation," J. Fluid Mech. **393**, 257 (1999).
[10] J. A. Johnson "The stability of shearing motion in a rotating fluid," J. Fluid Mech. **17**, 337 (1963).
[11] M. Lesieur, S. Yanase, and O. Métais, "Stabilizing and destabilizing effects of a solid-body rotation on quasi-two-dimensional shear layers," Phys. Fluids A **3**, 403 (1991).
[12] D. Tritton, "Stabilization and destabilization of turbulent shear flow in a rotating fluid," J. Fluid Mech. **241**, 503 (1992).
[13] P. Bartello, O. Métais, and M. Lesieur, "Coherent structures in rotating three-dimensional turbulence," J. Fluid Mech. **273**, 1 (1994).
[14] C. Cambon and L. Jacquin, "Spectral approach to nonisotropic turbulence subjected to rotation," J. Fluid Mech. **202**, 295 (1989).
[15] F. Waleffe, "Inertial transfers in the helical decomposition," Phys. Fluids A **5**, 677 (1993).
[16] C. Cambon, N. N. Mansour, and F. S. Godeferd, "Energy transfer in rotating turbulence," J. Fluid Mech. **337**, 303 (1997).
[17] Y. Morinishi, K. Nakabayashi, and S. Q. Ren, "Dynamics of anisotropy on decaying homogeneous turbulence subjected to system rotation," Phys. Fluids **13**, 2912 (2001).
[18] L. M. Smith and F. Waleffe, "Transfer of energy to two-dimensional large scales in forced, rotating three-dimensional turbulence," Phys. Fluids **11**, 1608 (1999).
[19] J. G. Charney, "Geostrophic turbulence," J. Atmos. Sci. **28**, 1087 (1971).
[20] P. Tabeling, "Two-dimensional turbulence: A physicist approach," Phys. Rep. **362**, 1 (2002).
[21] Y. Zhou, "A phenomenological treatment of rotating turbulence," Phys. Fluids **7**, 2092 (1995).
[22] V. M. Canuto and M. S. Dubovikov, "Physical regimes and dimensional structure of rotating turbulence," Phys. Rev. Lett. **78**, 666 (1997); "A dynamical model for turbulence. V. The effect of rotation," Phys. Fluids **9**, 2132 (1997).
[23] P. K. Yeung and Y. Zhou, "Numerical study of rotating turbulence with external forcing," Phys. Fluids **10**, 2895 (1998).
[24] Y. Hattori, R. Rubinstein, and A. Ishizawa, "Shell model for rotating turbulence," Phys. Rev. E **70**, 046311 (2004).
[25] C. N. Baroud, B. B. Plapp, Z.-S. She, and H. L. Swinney, "Anomalous self-similarity in a turbulent rapidly rotating fluid," Phys. Rev. Lett. **88**, 114501 (2002); C. N. Baroud, B. B. Plapp, H. L. Swinney, and Z.-S. She, "Scaling in three-dimensional and quasi-two-dimensional rotating turbulent flows," Phys. Fluids **15**, 2091 (2003).
[26] S. Galtier, "Weak inertial-wave turbulence theory," Phys. Rev. E **68** 015301(R) (2003).
[27] C. Cambon, R. Rubinstein, and F. S. Godeferd, "Advances in wave turbulence: rapidly rotating flows," New J. Phys. **6**, 73 (2004).
[28] M. Hossain, "Reduction in the dimensionality of turbulence due to a strong rotation," Phys. Fluids **6**, 1077 (1994).
[29] X. Yang and J. A. Domaradzki, "Large eddy simulations of decaying rotating turbulence," Phys. Fluids **16**, 4088 (2004).
[30] F. Bellet, F. S. Godeferd, J. F. Scott, and C. Cambon, "Wave-turbulence in rapidly rotating flows," in *Advances in Turbulence X*, edited by H. I. Andersson and P. A. Krogstad, 10th European Turbulence Conference (CIMNE, Barcelona, 2004).
[31] J. E. Ruppert-Felsot, O. Praud, E. Sharon, and H. L. Swinney, "Extraction of coherent structures in a rotating turbulent flow experiment," Phys. Rev. E **72**, 016311 (2005).
[32] O. Praud, J. Sommeria, and A. M. Fincham, "Decaying grid turbulence in a rotating stratified fluid," J. Fluid Mech. (to be published).
[33] P. Constantin, "Energy spectrum of quasigeostrophic turbulence," Phys. Rev. Lett. **89**, 184501 (2002).
[34] M. S. Mohamed and J. LaRue, "The decay power law in grid-generated turbulence," J. Fluid Mech. **219**, 195 (1990).
[35] LaVision GmbH, Anna-Vandenhoeck-Ring 19, D-37081 Goettingen, Germany.
[36] C. Kloosterziel and J. F. van Heijst, "An experimental study of unstable barotropic vortices in a rotating fluid," J. Fluid Mech. **223**, 1 (1991).
[37] C. Mutabazi, C. Normand, and J. E. Wesfreid, "Gap size effects on centrifugally and rotationally driven instabilities," Phys. Fluids A **4**, 1199 (1992).
[38] L. Zavala Sansón and G. J. F. van Heijst, "Nonlinear Ekman effects in rotating barotropic flows," J. Fluid Mech. **412**, 75 (2000).
[39] J. N. Gence and C. Frick, "Naissance des corrélations triples de vorticité dans une turbulence statistiquement homogène soumiseà une rotation," C. R. Acad. Sci. Série IIB **329**, 351 (2001).
[40] J. M. Foucault, J. Carlier, and M. Stanislas, "PIV optimization for the study of turbulent flow using spectral analysis," Meas. Sci. Technol. **15**, 1046 (2004).
[41] U. Frisch, *Turbulence* (Cambridge University Press, Cambridge, 1995).
[42] E. Lindborg, "Correction to the four-fifths law due to variations of the dissipation," Phys. Fluids **11**, 510 (1999).
[43] A. Belmonte, W. I. Goldburg, H. Kellay, M. A. Rutgers, B. Martin, and X. L. Wu, "Velocity fluctuations in a turbulent soap film: The third moment in two dimensions," Phys. Fluids **11**, 1196 (1999).
[44] C. Simand, F. Chillà, and J.-F. Pinton, "Inhomogeneous turbulence in the vicinity of a large-scale coherent vortex," Europhys. Lett. **49**, 336 (2000); "Inhomogeneous turbulence in the vicinity of a large-scale coherent vortex: erratum," *ibid.* **49**, 821 (2000).
[45] G. Boffetta, A. Celani, and M. Vergassola, "Inverse energy cascade in two-dimensional turbulence: Deviations from Gaussian behavior," Phys. Rev. E **61**, R29 (2000).
[46] S. A. Orszag, "Analytical theories of turbulence," J. Fluid Mech. **41**, 363 (1970).
[47] J. Y. Park and M. K. Chung, "An analytical model of velocity-derivative skewness of rotating homogeneous turbulence," Fluid Dyn. Res. **26**, 281 (2000).